VIBRATION ENERGY HARVESTING USING PIEZOELECTRIC TRANSDUCERS AND RECTIFIER CIRCUITS

Daniel Motter, daniel.motter@hotmail.com
Jairo Vinícius Lavarda, jairolavarda@gmail.com
Felipe Aguiar Dias, felipeaguiardias9@hotmail.com
Samuel da Silva, samsilva@unioeste.com
Western Paraná State University, UNIOESTE, Centro de Engenharias e Ciências Exatas, Av. Tarquínio Joslin dos Santos, 1300, 85870-900, Foz do Iguaçu, Paraná, Brazil

Vibration energy harvesting is of practical interest because of the demand for wireless sensing devices and low-power portable electronics without external power supply. Piezolectric transducers (PZT) are able to convert mechanical vibrations into electrical energy through an electronic circuit coupled to the PZT for current regulation and power management. The dynamic interactions between the mechanical structure, PZT, and the circuit are strongly influenced by the coupling. Several analytical and numerical models are available to estimate the output power of the system. Unfortunately, most of these models focused on simplifying the energy harvesting circuit into a simple resistive load. In the real-world applications, the energy harvesting circuit attached is more complex than a simple resistor. In this sense, the goal of the present paper is to develop a model of the PZT power harvesting device to estimate the output power provided by a beam coupled with a standard rectifier circuit. The fundamental single-mode resonance vibration under base excitation of a beam is used in the tests. The true electrical components were considered in the full-wave rectifier circuit with four diodes in bridge. A very simple and comprehensive description for choosing the capacitance and resistance loads is provided. In order to illustrate the results, numerical simulations and experimental verifications are also performed to ensure the accuracy.
Keywords: *smart structures, piezolectric transducers, energy harvesting, rectifier circuit.*

1. INTRODUCTION

Nowadays, the demand for portable, low-power, small electronic devices with a long-life battery has been increased, especially in cases where the battery replacement is difficult, requiring a system to recharge in real-time. Power harvesting systems with piezoelectric transducers, mainly PZT ceramics, can be effectively used for energy storage or to supply the load, where the energy is provided by environmental mechanical vibration.

Starner and Paradiso (2004) discuss the possibility of using alternative sources of vibration, such as the vibration of human breath captured through PZT in the human chest, and even recovery energy of blood pressure or provided by vibration when a person walk with shoes bonded with PZTs patches. Another very interesting study is the use of mechanical vibration caused by a raindrop when it touches the surface (Guigon *et al.*, 2008a,b). The experimental results validated a theoretical predictive model when the rain drops were at low speed. For high velocities of raindrop, the results differed because of an effect called *splash*, i.e. the drops result from a raindrop crashing against the piezoelectric ceramics.

For practical use, it is necessary to process the alternating current (AC) by using different rectifier circuits in order to charge batteries with direct current (DC). Several different rectifier circuits are widely shown in the literature, especially in the non-controlled and controlled circuits (Chagas *et al.*, 2010). Chagas *et al.* (2010), addressing the full-wave rectifier, showed that the electrical circuit connected to the transducer modifies the waveform in its terminals and claimed that the piezoelectric element becomes an open circuit only when the rectifier bridge is blocking, and the tension in the ceramic is less than in charge. However, Wickenheiser and Garcia (2010) observed that the fullwave rectifier has a smothing capacitor to provide a tension approximately constant over the load. A Synchronized Switch Harvesting (SSH) has also been analyzed in the area of energy harvesting with PZT sensors. Also, a Synchronized Switch Harvesting on Inductor (SSHI) has been developed, taking up to 160% efficiency over standard rectifier (Lallart and Guyomar, 2008). Other studies show the possibility of using inductors for switching (Ammar and Basrour, 2006). These techniques of circuit switched consider that the frequency is constant with sinusoidal signal. However, there is a lack of studies concerning circuit switched with electrical noise, where the non-controlled rectifier circuits have advantages.

The impedance electrical rectifier circuit, PZT transductor, and mechanical structure, all coupled, are extremely important in modeling and improving the efficiency of energy harvesting in smart structures. Sodano *et al.* (2004b) claimed that the dynamic properties of the beam are altered due to the change of load impedance, because this is a decisive factor to obtain the maximum output power. In another paper, Sodano *et al.* (2004a) proposed a model to determine the vibration necessary to supply power to electronic devices. Liu *et al.* (2009) provides provided an analytical and graphical analysis equation relating the output power with the efficiency of the rectifier circuit, which shows how important is the step of rectifying and storing the electrical charge.

Thus, the aim of this paper is to evaluate and compare the experimental results and the results provided by a theoretical

model of a full-wave diode bridge attached directly to the cantilevered smart beam with base excitation to cause transverse vibrations. All numerical tests and results are described and detailed by using the Matlab® and the SimPower System® toolbox of the Simulink®.The experimental setup is driven through the use of a DSpace® 1104 data acquisition with Control Desk®. In order to show some features, it is provided a number of simulations to illustrate the approaches. At the end, the final remarks present suggestions for further research.

2. NON-PARAMETRIC MODEL OF PIEZOELECTRIC ENERGY HARVESTING BEAM

The cantilever smart beam with bimorph PZT patches used in the present paper is shown in Fig. 1. The PZT used is the model PSI-5H4E manufatured by Piezo Systems®, where w_H and w_L are the width of the top and bottom PZTs, respectively, and t_t is the thickness.

The goal is only to describe it by using experimental data, a non-parametric model which is representative of the dynamics of the beam. Thus, a non-parametric model, the frequency response function (FRF), is obtained from spectral analysis.

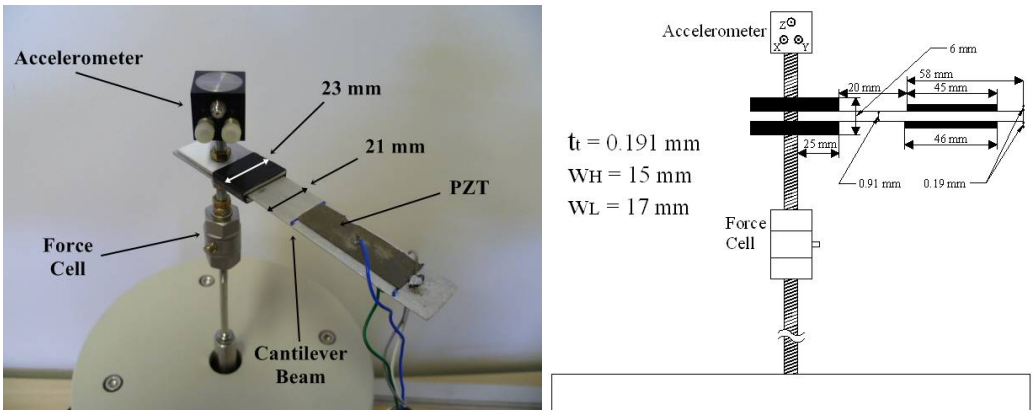

(a) Smart beam with shaker. (b) Schematic of beam describing the variables.

Figure 1. Smart beam attached to the shaker model TJ 50 TMC® and dimensions of beam when one end is clamped.

In order to determine the FRF of the system, an input chirp signal with frequency ranging from 0 to 2 kHz of lower PZT (actuator) was applied. The response on top PZT (sensor) of the beam connected in open circuit for measurement was recorded. The sampling rate used was 8 kHz and all acquisition was performed by using the DSpace® 1104 board controlled by the Control Desk® software. Figure 2 presents the result of the experimental FRF calculated by using the Welch method with 1500 samples, 50 % of overlapping and Hanning window.

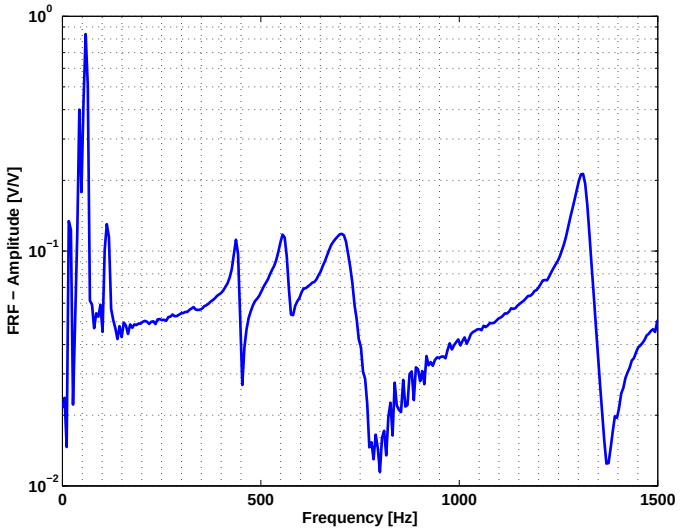

Figure 2. Frequency response function (FRF) of smart beam.

It is worth noting that at 58 Hz the system has a high peak gain, significantly greater than the other frequencies. Experimentally when a sinusoidal frequency with 58 Hz is applied in the shaker as input the level of vibration is high stating

and proving this is the first natural frequency of the beam. For monitoring the level of force applied and displacement in the beam two additional transducers were employed: a load cell, model TF-YD-312 TMC® with sensitivity of 3.02 pC/1 N, and an IEPE accelerometer TA-YD-193 TMC® with sensitivity of 1.007 mV/ms^{-2}. The measurements performed with this sensor were only qualitative.

3. MODEL OF ENERGY STORAGE CIRCUIT ATTACHED

Usually, in real-world application of vibration power harvesting, a rectifier circuit is necessary to convert AC to DC in order to charge a battery or to feed directly an electronic device. A very simple and common non-controlled rectier circuit is the full-wave rectifier with diode bridge. A schematic diagram is shown in Fig. 3.

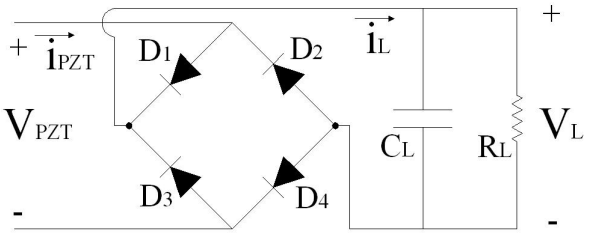

Figure 3. Esquematic diagram of full-wave bridge rectifier.

The non-controlled rectifier can transform an alternating signal continuously, but if a capacitor in parallel to the load is not employed, the output signal could have a considerable ripple, which may be unacceptable for powering loads with voltage DC. So, the circuit to supply a resistive load uses a capacitive filter which smooths the effect of voltage variation in load. The ripple was defined how the reason between the component AC for the component DC of the signal. The component DC of the signal is illustrated by the following equation, where t_f is the final time of measurement.

$$V_{avg} = \frac{\int_0^{t_f} v_L(t)\,dt}{t_f} \tag{1}$$

and the component AC is the relation of the signal and the DC level calculated by:

$$v_{L_{AC}}(t) = v_L(t) - V_{avg} \tag{2}$$

When the ripple is closer to zero (0%), more solid signal indicates a characteristic quality voltage DC. The next equation shows how the ripple is calculated:

$$V_{rms_{AC}} = \sqrt{\frac{\int_0^{t_f} v_{L_{AC}}^2(t)\,dt}{t_f}} \tag{3}$$

$$\textit{ripple}(\%) = \frac{V_{rms_{AC}}}{V_{avg}} \times 100 \tag{4}$$

where $V_{rms_{AC}}$ and V_{avg} are the RMS and average voltage, respectively. First, the average signal is calculated, and after subtracting from the original signal, taking only the AC voltage, the RMS value was calculated. This effect can be explained by analyzing the following equation:

$$\tau = RC \tag{5}$$

where the time constant capacitive τ represents the time which a RC circuit takes to charge or discharge. The current in this case varies in parallel RC circuit by:

$$i_r(t) = \frac{V_o}{R} e^{-\frac{t}{RC}} \tag{6}$$

where V_o is the voltage in steady state before discharge. Clearly, it is observed that the greater is C, more time is consumed to power the load in the form of electric field. On the other hand, the biggest the R, less power is consumed and thus less time it takes to discharge the circuit. In summary, higher the τ, the better the quality of the rectified signal and better your ripple.

The charge is given by:

$$q_{C_L} = C_L V_L \tag{7}$$

and energy stored:

$$E_C = \frac{1}{2} C_L V_L^2 \tag{8}$$

So, the energy in the capacitor is directly proportional to its capacitance C.
The internal transducer capacitance of the PZT without external load is given by:

$$C_p = \frac{\epsilon^T w_H L_{pH}}{t_t} + \frac{\epsilon^T w_L L_{pL}}{t_t} \tag{9}$$

where ϵ^T is the permittivity of PZT when the stress is constant [C^2/Nm^2], L_{pH} and L_{pL} is the length [m] of top and bottom PZT and w_L, w_H and t_t was defined previously, with the distances given by Fig. 1(b). The permittivity in vacuum is $\epsilon_o = 8.854e-12$ [C^2/Nm^2], K = 3400 given by the PZT manual used for the PZT PSI-5H4E and with the relationship $\epsilon^T = \epsilon_o K$, the value of this capacitance calculated is $C_p = 229.64$ nF.

Now, the resistor R_L is chosen by considering that it does not significantly affect the output voltage ripple, causing the capacitive load time is significantly longer than the period of the signal voltage at the terminals of the PZT transducer. If the circuit has low resistance value R_L, the constant τ is small, and the discharge of the $R_L C_L$ parallel circuit would be faster than the voltage to reach zero value. Finally, the instantaneous power consumed by the load is directly proportional to the square of the voltage and inversely proportional to resistance and the active power consumed by the resistor and can be calculated by:

$$P_{L_{avg}} = \frac{V_{avg}^2}{R_L} \tag{10}$$

4. NUMERICAL AND EXPERIMENTAL RESULTS

The tests performed in order to illustrate the approach proposed are presented in this section. The basic procedure proposed in this paper consists of several steps. Firstly, the schottky diode 1N5817 is experimentally characterized in order to provide a correct numerical simulation. Subsequently, the procedure for choosing the values of resistance R_L and capacitance C_L used in the rectifier circuit is described. The comparison between the numerical and experimental performance for different levels of vibration and frequency is then presented. The section is concluded with a very simple example to show the applicability and effectiveness of the experimental setup to light a LED.

4.1 The curve of the diode 1N5817

It is well known that the schottky and germanium diodes have forward voltage drop significantly lower than silicon diodes. The 1N5817 schottky diode was chosen after checking many datasheets of components seeking to chose the lower forward voltage drop, so that the voltage drop was the minimum possible. The full-wave rectifier circuit was simulated by using the Simulink® since the non-linear behavior of the diode can be easily verified with this software. An experimental test was performed to identity the relationship between current and voltage in the 1N5817 schottky diode. Figure 4 illustrates the experimental setup used to determine the current *versus* voltage curve by using a DC source, a diode and a resistor of 10kΩ.

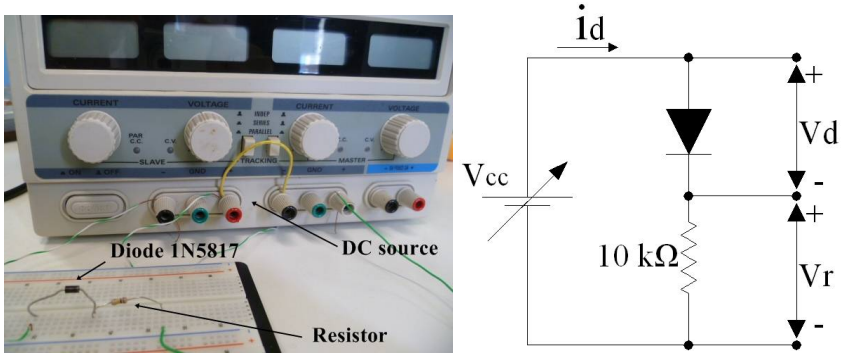

(a) Experimental setup. (b) Schematic test circuit.

Figure 4. Circuit for experimental identification of the current *versus* voltage curve.

The value of 10kΩ was chosen to the test so that only low currents cross the diode element, because power harvesting applications in smart structures have small amounts of current (order of mA). The voltage across the resistor was measured

with the DSpace® 1104 and the current was determined indirectly by the relationship $V_r = RI_d$. If the data acquisition of the voltage of the DC source is performed, the relationship can be easily calculated by $V_d = V_{cc} - V_r$ and the voltage-current curve is obtained. Figure 5 presents the result of the experimental voltage curve of the diode and another one identified by using a polynomial. A representative curve was used to identify the forward voltage drop, $V_j = 50$ mV, and internal resistance of the diode, $r_d = 280\Omega$, which represents the slope of the curve after the voltage V_j.

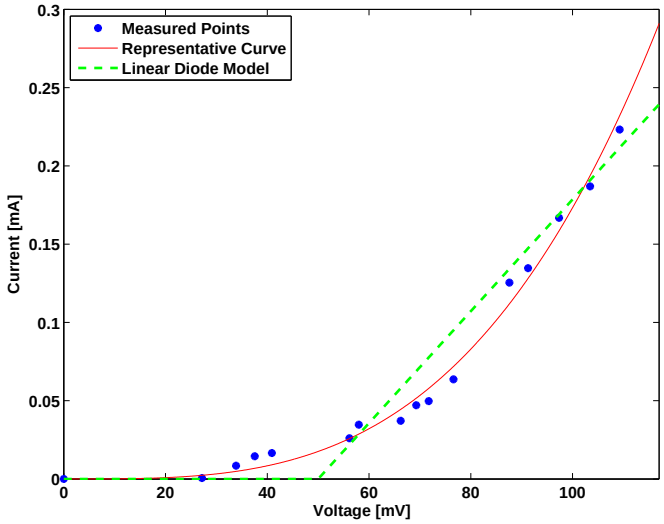

Figure 5. Current *versus* Voltage curve of the diode $1N5817$.

4.2 Desgin of the load C_L and R_L

The design of the capacitance load C_L of full-wave rectifier circuit is based on the criterion of time charging, level of voltage provided on the load and stored energy in the form of electric field. It is also assumed that the resistor R_L is an open circuit (infinity value). A sinusoidal signal of excitation of amplitude 0.5 V was applied on the Thevenin source voltage. Figure 6(a) shows the experimental rectifier circuit implemented on a protoboard. The smart beam with PZT is numerically simulated trough a Thevenin source voltage with a PZT capacitance C_p calculated by Eq. (9). The Simulink® software with the SimPower System® toolbox is used to perform numerical simulations, Fig 6(b), where the parameters V_j were r_d used to simulate the diodes. The frequencies used in the test were set based on Fig. 2, 58 Hz and 437 Hz. The 58 Hz is the first natural frequency with the greatest intensity of vibration in the beam. The natural frequency of 437 Hz is used only to compare the results. Fig. 7 presents the assessment of capacitive load in the diode bridge for both frequencies.

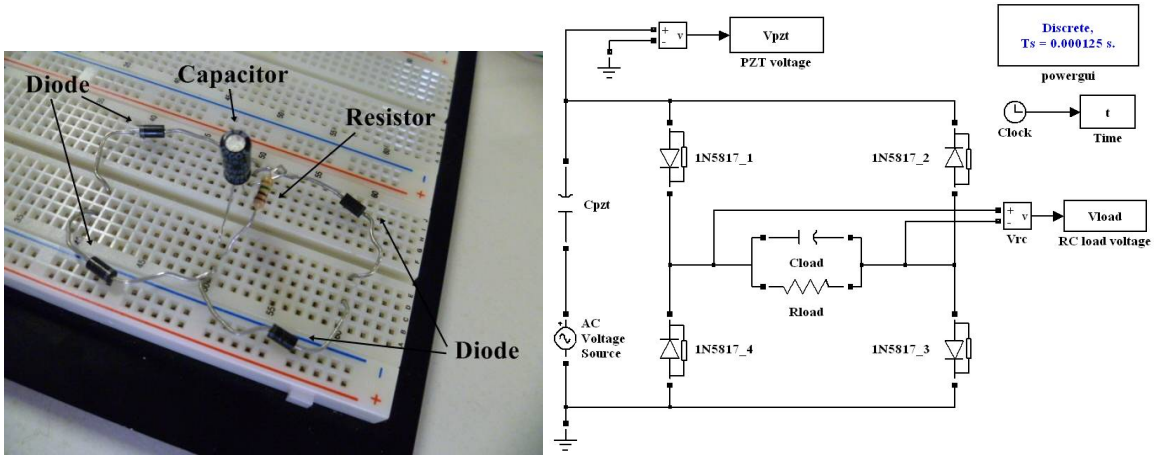

(a) Experimental rectifier circuit implemented on a protoboard. (b) Schematic of the rectifier circuit implemented in the Simulink®.

Figure 6. Full-wave bridge rectifier.

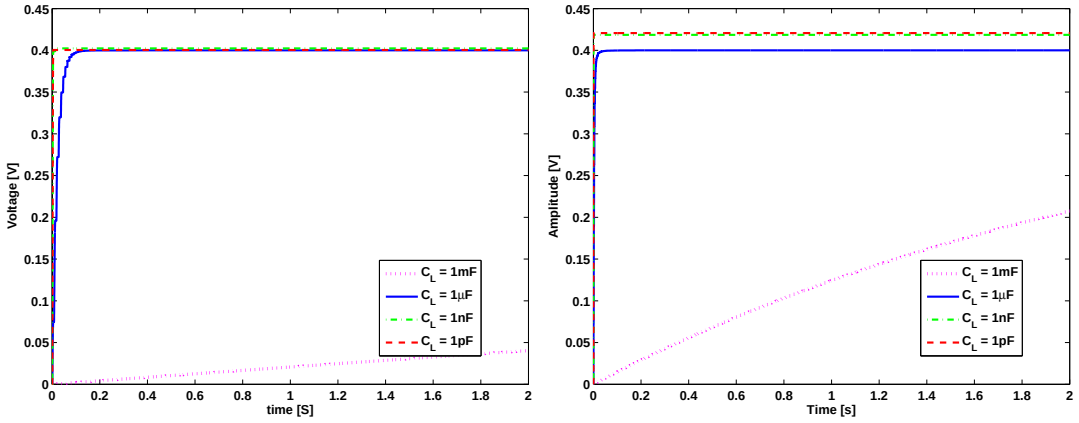

(a) 58 Hz. (b) 437 Hz.

Figure 7. Assessment of capacitive load in the diode bridge.

As one can observe above for both frequencies the load capacitance of $C_L = 1$ mF takes longer to reach the steady state, but without completing the load. The other capacitances reach the steady state before with almost the same voltage in both. Since both capacitors reach the steady state with the same voltage level, one can use Eq. (8) to chose the capacitance to provide the greater energy stored in the form of electric field. Thus, it is determined that the load capacitor with $C_L = 1\mu$F is a right choice for both frequencies of 58 and 437 Hz, even where the voltage is lower. For the frequency of 437 Hz and when the $C_L = 1$ μF, the steady voltage amplitude is $V_L = 0.4$ V and $E_L = 80$ nJ calculated by Eq. (8). For $C_L = 1$ nF the steady voltage amplitude is $V_L = 0.419$ V and $E_L = 87.6$ pJ. Finally, for $C_L = 1$ pF, the steady amplitude is $V_L = 0.42$ V and $E_L = 0.088$ pJ. Thus, the capacitance of $C_L = 1$ μF is a viable chose, even with the low level of voltage amplitude, the level of energy and the current provided is bigger when compared to the other capacitance values tested.

Another important task is to choose an appropriate resistive load R_L to consume the active power. This passive element represents an electronic device and is designed to maintain a certain amount of ripple and voltage level measured at its terminals. It is also necessary to consider that the power consumed is directly proportional to the square of the voltage and inversely proportional to resistance. The same voltage input signal was applied to the source, but now the resistor is not an open circuit. Table 1 presents the average values of voltage, RMS voltage of AC ripple and resistance to different values. The frequencies of 58 Hz and 437 Hz were assumed, as well as, the same capacitance C_L and AC voltage source.

Table 1. R_{Load} assessment.

Frequency [Hz]	R_{Load} [Ω]	V_{avg} [V]	$V_{rms_{AC}}$ [V]	Ripple [%]	$P_{L_{avg}}$ [μW]
58	1 kΩ	0.020	0.012	61.175	0.417
58	1 MΩ	0.387	0.028	7.353	0.150
58	1 GΩ	0.396	0.029	7.432	0.000
58	1 TΩ	0.396	0.029	7.433	0.000
437	1 kΩ	0.103	0.016	15.553	10.552
437	1 MΩ	0.395	0.011	2.838	0.156
437	1 GΩ	0.399	0.011	2.860	0.000
437	1 TΩ	0.399	0.011	2.860	0.000

Analyzing the results in Tab. 1, it is observed that the higher the resistance value R_L, the ripple voltage is lower and the load voltage is greater. The increase of the voltage load is caused by the increase of R_L, because the implementation of C_L and R_L parallel increases too, and C_p is still the same, causing a greater voltage on the load. The ripple decreases because the τ increases as the resistance increases, causing the discharge signal to smooth. For both frequencies, the resistors with resistance of 1 MΩ, 1 GΩ and 1 TΩ have approximately the same ripple and average voltage, but as P_L of the resistor 1 MΩ is bigger, this value is the chosen one. Therefore, the resistance chosen is 1 MΩ for the frequencies of 58 Hz and 437 Hz with a capacitive load of $C_L = 1\mu$F in parallel to $R_L = 1$ MΩ. It is worth noting that the Tab. 1 shows only same resistance candidates for the best value by considering ripple V_{avg} and P_{avg} power consumed by the load. The values R_L could be refined to find better parameters, e. g., by simulating a resistance of $R_L = 500$ kΩ and observing, if the ripple, V_{avg} and P_{avg} improve as a function of the parameter concerned. The same consideration can be performed to choose the C_L.

4.3 Experimental results

The experimental test of the power harvesting device designed is performed by using a modal shaker TJ 50 TMC®, where the smart beam is attached, a power amplifier TE $5874A$ TMC®, sweeping and sinusoidal signal generator TE $1311E$ TMC®, DSpace® 1104 data acquisition board controlled by Simulink® and Control Desk® software and a proto-board to attach the circuit designed. Figure 8 shows the complete experimental setup utilized in the tests with a schematic diagram.

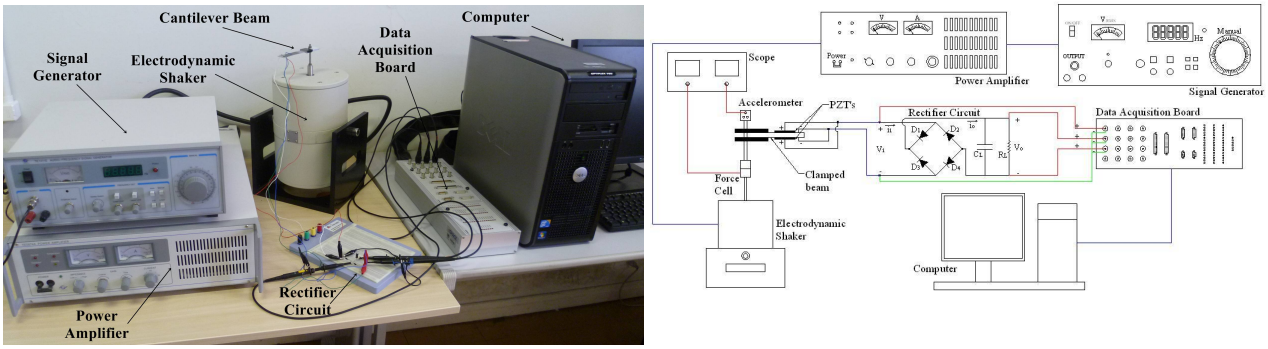

(a) View of the equipaments used. (b) Schematic diagram.

Figure 8. Experimental setup.

The beam has two PZTs coupled, and the ceramics have been connected in parallel. The full-wave rectifier circuit was composed of four 1N5817 diodes, resistor, and electrolytic capacitor, as described before. In all tests of this section, the output voltage data in PZT and in the load C_L were recorded with a sampling rate of 8 kHz and with 16001 samples in each file, being measured during two seconds. In order to monitor the level of displacement and force applied in the beam an oscilloscope was employed to measure these parameters.

Figure 9 presents the comparison between the numerical and experimental test. The simulation was performed with Simulink®, Fig. 6(b), and by using the peak value of sinusoidal voltage source of 0.43V, measured experimentally. In the Simulink®, the *ode23t* (Mod. stiff/Trapezoidal) command is used as solver with variable time step.

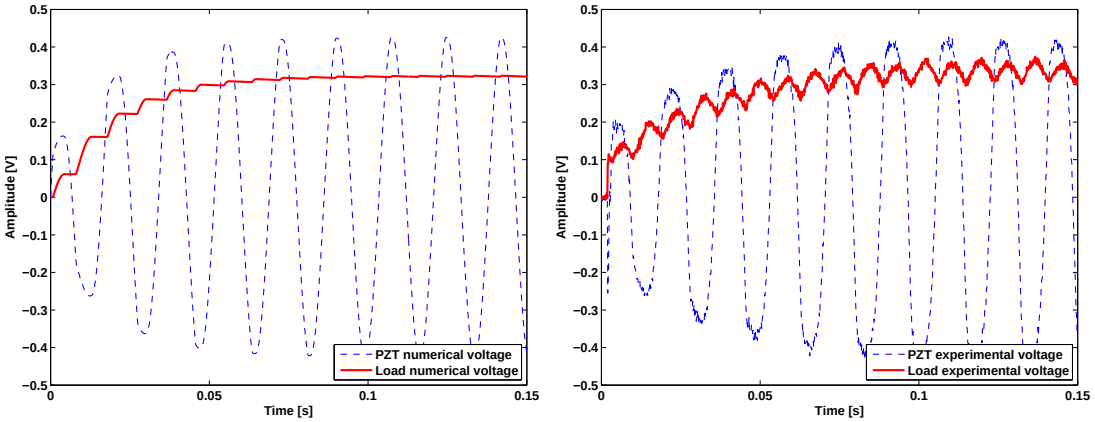

(a) Numerical. (b) Experimental.

Figure 9. PZT and load voltage for transitory condition with 58 Hz.

Now using the excitation frequency of 437 Hz, the same test was done. The value of force was set by using the gain in the power amplifier to supply the shaker in order to reach a level of 0.47 V in the PZT. The voltage magnitude across the PZT to the frequency of 58 Hz and 437 Hz are different because the highest possible gain has been avoided before the accelerometer signal becomes noisy. Figure 10 presents the comparison between the numerical and experimental test.

Figure 11(a) and 11(b) indicates the experimental PZT and load voltage for the steady condition of the frequencies of 58 Hz and 437 Hz, respectively.

Finally, a direct comparison between the load voltages obtained experimentally and numerically are shown in Fig. 12 for both frequencies. The level of voltage and the general behavior are well simulated with the mathematical model provided by Simulink®. However, it is clear that the experimental ripple is greater. The diode is simulated by static representation, as a resistance in series with a DC voltage source, where the real circuit highlights the dynamic characteristics

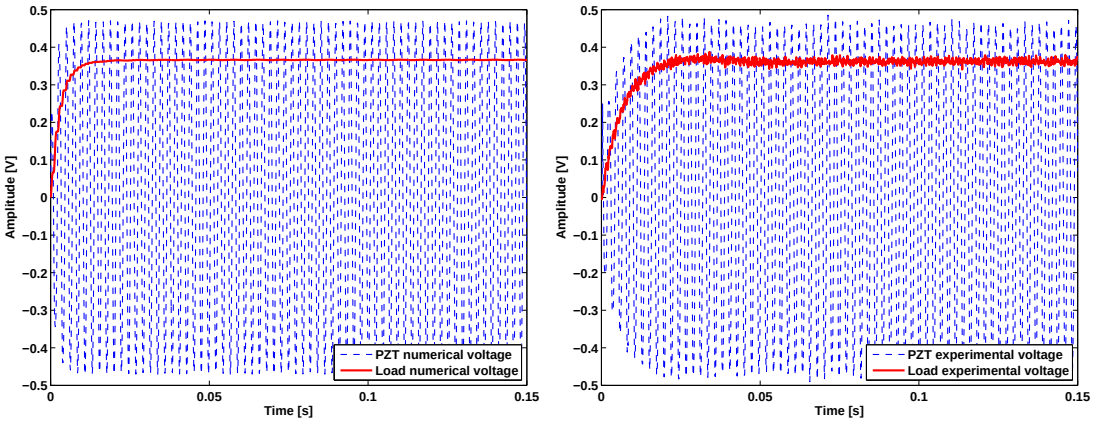

(a) Numerical. (b) Experimental.

Figure 10. PZT and load voltage for transitory condition with 437 Hz.

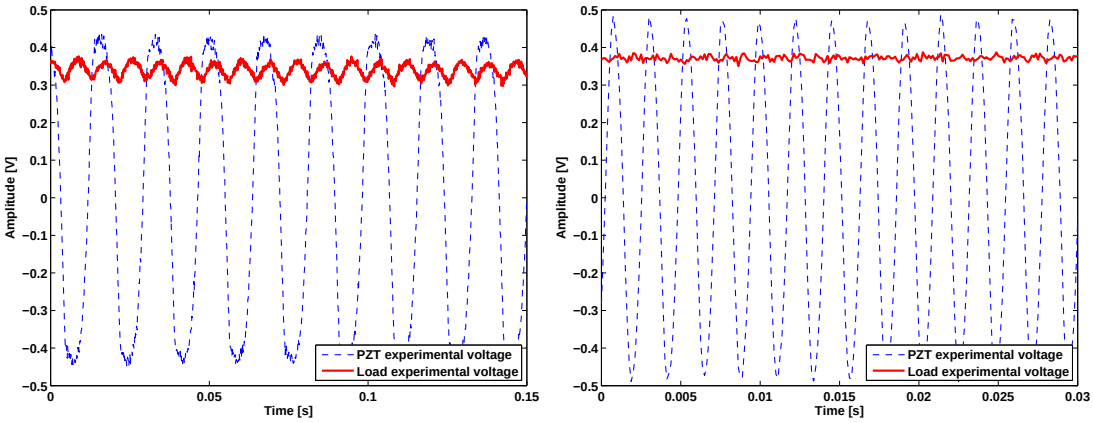

(a) 58 Hz. (b) 437 Hz.

Figure 11. Experimental PZT and load voltage for steady condition.

of the diode, including non-linearity of this component. As the curve shows different points of slope (and thus resistance), the static modeling loses some information. The ripple is presented as something dynamic that is not to be represented in static form, but the DC voltage level had good representation. So, a better model updating is wished in the next tests. Another point is relative to compare other numerical methods to solve the non-linear equations in the rectifier circuits.

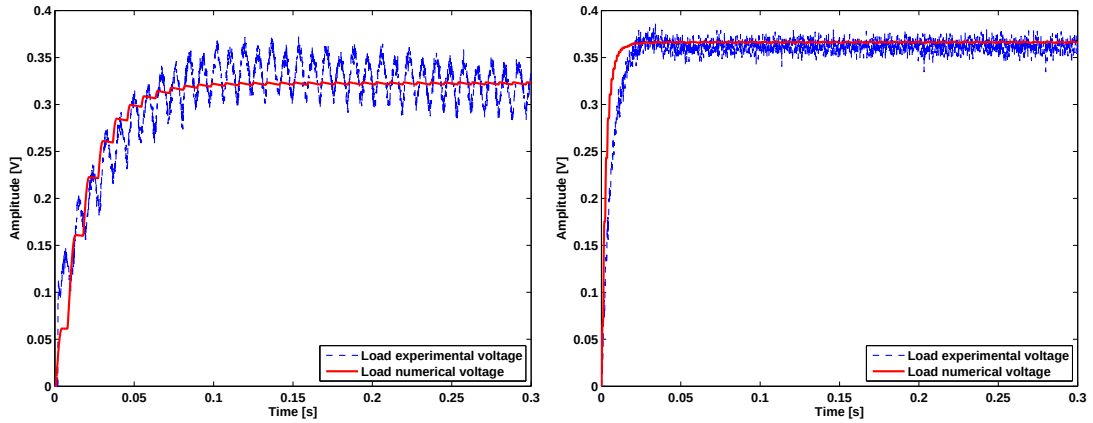

(a) 58 Hz. (b) 437 Hz.

Figure 12. Load voltage comparison.

4.4 Application

The power harvesting device is tested for a possible application as an indicator of the level of charging in a battery. An Light-Emitting Diode (LED) is installed parallel to a capacitor to indicate when the charge in the capacitor reaches the adequate value of voltage. If the LED on, the capacitor voltage reaches a minimum level expected and, consequently, the stored charge can be calculated by Eq. (7). Two sets of test were realized to lighting the LED. For both tests, the load is $C_L = 3300$ μF, R_L is the LED and a sampling rate of 2 kHz is used. These tests, were recorded with a sampling rate of 2 kHz and with 200001 samples per file, being measured by one hundred seconds.

The aim of the first analysis is to compare the time of loading and the voltage level on the capacitive load when the excitation signal has the frequency equals the first natural frequency of 58 Hz and to the natural frequency of 437 Hz. The gain in the power amplifier to suppy the modal shaker is maintained constant in both cases. Figure 13(a) shows the voltage across the LED (and capacitor) for different frequency values, but keeping the fixed applied force. The displacement in the clamped of the beam for 58 Hz was higher than the frequency of 437 Hz, and the LED on for about 120 seconds. For the frequency of 437 Hz, after a wait of 6 minutes the LED is still not lit.

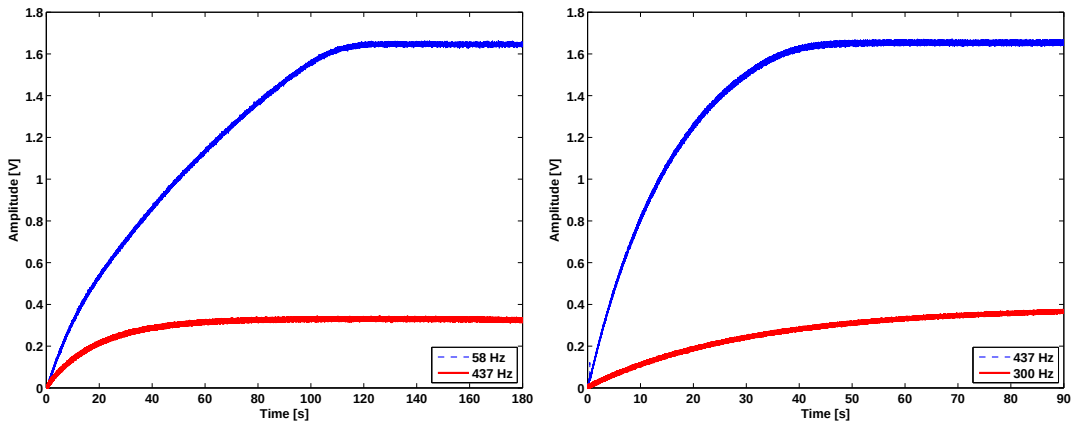

(a) Ressonance Frequency Comparasion. (b) Simple Frequency Comparasion.

Figure 13. Time of loading and the voltage level on the capacitive load for different frequency and level of force amplitude.

The second analysis performed the same comparison, but by considering a ressonance frequency of 437 Hz and any other frequency, like 300 Hz. Figure 13(b) presents the results of the load voltage for both frequencies, where the same level of force was applied corresponding to approximately three times of the first analysis. For this value of force at 437 Hz, the LED on for about 50 seconds. Clearly, the first ressonance frequency is better to charge the load. Now, for the frequency of 300 Hz, after a wait of 6 minutes the LED is not lit. The Figure 13(b) shows the cases in which the LED in the circuit is on or off. Figure 14 illustrates the application when LED is off and on.

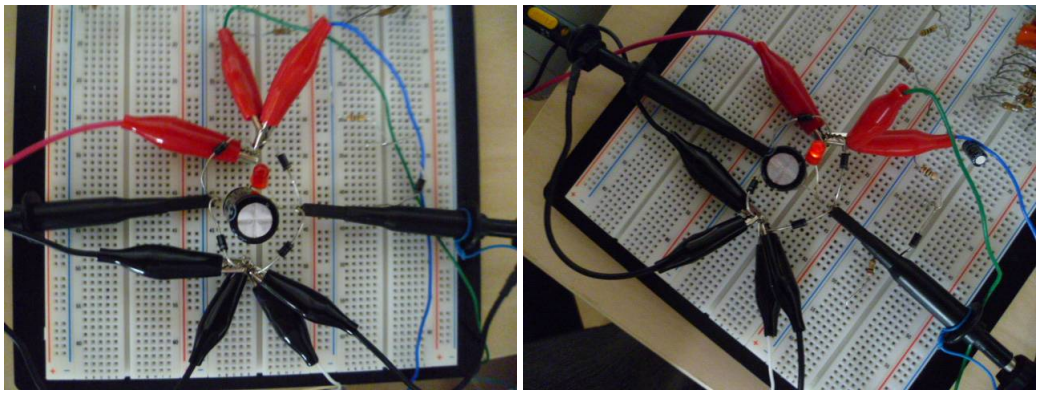

(a) LED off. (b) LED on.

Figure 14. Power harvesting device to light an LED.

5. FINAL REMARKS

Vibration power harvesting represents a huge potential for commercial applications in different areas, as presented in recent researches, mainly in networks for structural health monitoring (SHM). In this sense, this paper illustrated the applicability and some aspects for a fast and simple design of a device for practical application. It was shown through several experimental tests that the higher the load resistance, greater the voltage magnitude. However, as the higher the resistive load, the lower the power consumed by the load, thus the performance for a practical application that requires a level of considerable power will be difficult. The greater the capacitance of the load C_L, more time is required to charge the capacitor. However, the ripple is bigger and the τ is shorter, causing a discharge faster. Another important point is to choose an adequate value of excitation frequency, mainly in the first natural frequencies where the level of vibration amplitude can be bigger. Usually, the mechanical beam design is based on the information about the real-world mechanical source, e.g. a machine or a structural frame. Further research is being developed by the authors to reach a mathematical model of the mechanical vibration of the beam with multiple modes attached to the non-controlled rectifier circuits considering the same software package (Simulink®), in order to provide the information needed for this design.

6. ACKNOWLEDGEMENTS

The authors would like to thank for the financial support provided by National Council for Scientific and Technological Development (CNPq/Brazil), Grant no. 301582/2010-6, Fundação Araucária, Grant no. 15997/2010, and SETI-PR. Daniel Motter and Felipe Aguiar Dias are thankful their scholarships from Parque Tecnológico Itaipu (PTI/Brazil). Jairo Vinícius Lavarda is thankful his scholarship from PIBIC/CNPq.

7. REFERENCES

Ammar, Y. and Basrour, S., 2006. "Non-linear techniques for increasing harvesting energy from piezoelectric and electromagnetic micro-power-generators". In *DTIP of MEMS & MOEMS*.

Chagas, M.C.O., Neto, R.M.F. and Gallo, C.A., 2010. "Revisões dos circuitos derivativos e suas variações usadas na regeneração de energia a partir de materiais piezoelétricos em estruturas vibrantes (2006-2009)". In *VI National Congress of Mechanical Engineering*.

Guigon, R., Chaillout, J.J., Jager, T. and Despesse, G., 2008a. "Harvesting raindrop energy: experimental study". *Smart Materials and Structures*, Vol. 17, p. 015039 (6pp).

Guigon, R., Chaillout, J.J., Jager, T. and Despesse, G., 2008b. "Harvesting raindrop energy: theory". *Smart Materials and Structures*, Vol. 17, p. 015038 (8pp).

Lallart, M. and Guyomar, D., 2008. "An optimized self-powered switching circuit for non-linear energy harvesting with low voltage output". *Smart Materials and Structures*, Vol. 17, p. 035030 (8pp).

Liu, Y., Tian, G., Wang, Y., Lin, J., Zhang, Q. and Hofmann, H.F., 2009. "Active piezoelectric energy harvesting: General principle and experimental demonstration". *Journal of Intelligent Material Systems and Structures*, Vol. 20, pp. 575 – 586.

Sodano, H.A., Park, G. and Inman, D.J., 2004a. "Estimation of electric charge output for piezoelectric energy harvesting". *Strain*, Vol. 40, pp. 49 – 58.

Sodano, H.A., Inman, D.J. and Park, G., 2004b. "A review of power harvesting from vibration using piezoelectric materials". *The Shock and Vibration Digest*, Vol. 36, pp. 197–205.

Starner, T. and Paradiso, J.A., 2004. "Human generated power for mobile electronics". In *Low Power Electronics Design*.

Wickenheiser, A. and Garcia, E., 2010. "Power optimization of vibration energy harvesters utilizing passive and active circuits". *Journal of Intelligent Material Systems and Structures*, Vol. 21, pp. 1343–1361.

8. Responsibility notice

The authors are the only responsible for the printed material included in this paper.